sciendo
ISSN 1335-8871
MEASUREMENT SCIENCE REVIEW

Analysis of Coupled Vibration Characteristics of Linear-Angular and Parameter Identification

Bo Tang[1, 2*], Jiangen Yang[1], Wei Chen[2], Xu Ming[1]

[1]*Metrology and Measurement Engineering, China Jiliang University, Xueyuan Street, No.258, 310018, Hangzhou, China, tangbo@cjlu.edu.cn*
[2]*Ningbo Water Meter (Group) Company Ltd., Hongxing Road, No.355, Ningbo, 315032, China*

Abstract: A steady-state sinusoidal and distortion-free excitation source is very important for the accuracy and consistency of the calibration parameters of micro-electro-mechanical systems (MEMS) inertial sensors. To solve the problem that the current MEMS inertial measurement unit (IMU) calibration device is unable to reproduce the spatial motion of linear and angular vibration coupling, research topics on the coupling vibration characteristics and parameter identification for an electromagnetic linear-angular vibration exciter are proposed. This research paper used Ampere's law and Lorentz force to establish the analytical expressions for the electromagnetic force and electromagnetic torque of the electromagnetic linear-angular vibration exciter. Then, the main purpose of this paper is to establish uniaxial and coupled vibration electromechanical analogy models containing mechanical parameters based on the admittance-type electromechanical analogy principle, and the parameter identification model is also obtained by combining the impedance formula with the additional mass method. Finally, the validity of the coupling vibration characteristics and the parameter identification model are verified by the frequency response simulation and the additional mass method, and the relative error of each parameter identification is within 5% in this paper.

Keywords: Vibration exciter, linear-angular vibration, vibration characteristics, parameter identification, electromechanical analogy.

1. INTRODUCTION

In recent years, with the rapid development of micro-electro-mechanical systems (MEMS) inertial sensors, attention has been paid to the exciters used for MEMS inertial sensor calibration, and higher requirements have been placed on the output performance of the exciters [1]. Traditional sensor calibration methods often use electromagnetic exciters [2], and compared to uniaxial vibration excitation, linear-angular composite vibration excitation can simulate the actual dynamic environment more accurately. An electromagnetic linear-angular vibration exciter can not only output uniaxial linear vibration and angular vibration, but also has the function of outputting linear and angular vibration synchronously. However, there is coupling vibration when the exciter synchronously outputs linear-angular vibration, the research on exciter vibration has mostly focused on uniaxial vibration, and research on its linear and angular vibration has been conducted independently [3] without considering the correlation between the two types of vibration. The independent research of vibration forms can certainly simplify the problem, but it separates the inherent connection and cannot reflect the actual vibration situation of the propulsion axis system.

The operating principle of the electromagnetic linear-angular vibration exciter is that the moving coil generates an ampere force in the magnetic field, which drives the moving part to emit vibration. Therefore, it can be divided into two aspects: electromagnetics and dynamics. As for electromagnetics, a closed magnetic field must be established in different directions in the air gap of the exciter to generate linear and angular vibration at the same time, and current must flow in different directions in the moving coil. Based on Ampere's law, an electromagnetic force and torque are simultaneously applied to the coil, and the moving parts are excited by the Ampere force generated by the coil to generate vibration. However, multi-axis vibration may cause the vibration of the moving part to be eccentric, resulting in mutual influence between the two vibration modes, generating coupled vibration [4]. And the coupled vibration caused by the deflection may lead to fatigue, fracture and friction problems in the internal structure of the exciter, which will affect the overall performance of the exciter [5]. Therefore, the study of the coupled vibration characteristics of this exciter has important engineering significance. With the attention and recognition of the influence of coupled vibration on machinery, research on coupled vibration has gradually developed in recent years. Researchers have studied a large number of analysis methods, such as the energy method, the transfer matrix method, the finite element method, and the wave approximation method [6]. In recent years, many scholars have conducted research on the establishment of coupled vibration models. Huang [7] established a lumped parameter model based on the coupled

DOI: 10.2478/msr-2024-0003
**Corresponding author: tangbo@cjlu.edu.cn (B. Tang)*

torsional-longitudinal vibration phenomenon of ship propellers and conducted numerical simulations and experimental tests based on the proposed model. The results showed that the natural frequency is not affected when the maximum acceleration increases with increasing speed and load.

The dynamic model parameters are the basis for a precise analysis of the dynamic properties of the vibration system of the exciter. Therefore, the identification of the coupling vibration parameters of an electromagnetic linear-angular vibration exciter has important engineering significance [8]-[9]. Modal analysis is an important method for parameter identification of mechanical structures. By establishing a modal model of the structure and combining it with experiments, the dynamic parameters of the structure can be identified [10]. Wen [11] identified the modal parameters of a double-curved cable-stayed bridge through forced vibration experiments, and calculated the modal parameters based on frequency response curves under the different excitation conditions. Song [12] used a modal parameter identification method based on experimental vibration data to estimate the parameters of a concentrated mass mechanical system in a vibration experiment. However, the structure of the electromagnetic linear-angular vibration exciter is relatively complex and the analysis process is more cumbersome. Since the electromagnetic exciter has both mechanical and electrical systems and the mathematical models of the mechanical and electrical systems are essentially the same, the use of the electromechanical analogy theory to analyze complex shaker vibration systems can greatly simplify the analysis process [13]. In the research on the application of electromechanical analogy to parameter identification, Saraswat [14] established a lumped parameter model for the electromagnetic vibration screening system and developed a parameter identification model for the electromagnetic vibration screen based on the electromechanical analogy, which takes into account the nonlinearity of the system. Based on the lumped parameter model for the electromagnetic uniaxial exciter, Tiwari [15] established the identification model of the key parameters of the exciter based on modal analysis and combined with the principle of electromechanical analogy.

This article focuses on the study of the coupling vibration characteristics during the operation of the electromagnetic linear-angular vibration exciter and proposes a parameter identification method suitable for this exciter. First, the electromagnetic force and electromagnetic torque models of the electromagnetic linear-angular vibration exciter are introduced and then their expressions are established. On this basis, the differential equations of motion for the uniaxial and coupled vibration of the exciter are established, and the coupling vibration characteristics are analyzed based on the vibration equations. Second, based on the principle of admittance-type electromechanical analogy, electromechanical analogy models for uniaxial and coupled vibration containing mechanical parameters are established. Based on the model, an impedance formula with dynamic parameters is derived and the identification model of its dynamic parameters is obtained by combining the additional mass method. Finally, the above conclusions on the vibration characteristics and the theoretical models are verified by simulations.

2. MODELS OF ELECTROMAGNETIC FORCE AND TORQUE

The dynamic properties of an electromagnetic linear-angular vibration exciter are analyzed. First, the analytical expressions for the electromagnetic force and the electromagnetic torque of the exciter are established. Then, a uniaxial and a coupled vibration model of the exciter are created based on these expressions. Fig. 1 shows the driving structure of the exciter, which mainly consists of permanent magnets, the inner core, the outer core, the moving coil (circumferential coil and axial coil), coil bobbin and the moving table.

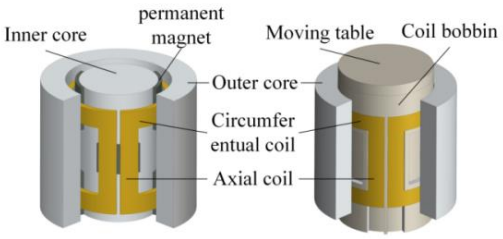

Fig. 1. The driving structure of the exciter.

Permanent magnets are radially magnetized and they stick to the outer wall of the inner core. It is arranged alternately in four equal parts along the circumference and three equal parts along the axis. The permanent magnets at the upper and lower ends along the axis and the inner and outer cores form a linear vibration air gap magnetic field, while the permanent magnets in the middle and the inner and outer cores form an angular vibration air gap magnetic field. The moving coil is divided into a circumferential and an axial part. The circumferential coil is located in the linear vibration air gap magnetic field and the axial coil in the angular vibration air gap magnetic field. After the moving coil has been energized with sinusoidal alternating current, circumferential coil emits an axial electromagnetic force and the axial coil an axial electromagnetic torque in accordance with the Lorentz force law. After the magnetic circuit and coil structure are determined, when the moving coil is energized with sinusoidal alternating current, the exciter generates a compound linear-angular vibration that varies with the current, and the electromagnetic force and electromagnetic torque are proportional to the moving coil current.

The analytical model expression of the air gap magnetic field is obtained based on the equivalent current method:

$$B_r = \frac{1}{r}\frac{\partial A_z}{\partial_\varphi} - \frac{\partial A_z}{\partial_z} =$$
$$\frac{\mu_0 M}{4\pi}\sum_{j=1}^{2}(-1)^{(j+1)} \times \{\int_{r(1)}^{r(2)}\int_{\varphi(1)}^{\varphi(2)} \frac{(z-z(j))\cos(\varphi-\varphi')}{\left[r^2+r'^2-2rr'\cos(\varphi-\varphi^1)+(z-z(j))^2\right]^{\frac{3}{2}}} \mathrm{d}\varphi'\,\mathrm{d}r' +$$
$$+\int_{r(1)}^{r(2)}\int_{z(1)}^{z(2)} \frac{\sin(\varphi-\varphi(j))r'}{\left[r^2+r'^2-2rr'\cos(\varphi-\varphi(j))+(z-z')^2\right]^{\frac{3}{2}}} \mathrm{d}z'\,\mathrm{d}r' \tag{1}$$

where B is the MFD, A is the magnetic potential, μ_0 is the permeability of the vacuum, M is the magnetization.

The radial magnetic induction intensity generated by each permanent magnet is calculated separately. Based on the position relationship between the permanent magnets and the

magnetization direction of each permanent magnet, the analytical model expression of the magnetic field structure can then be obtained by superimposing the magnetic fields generated by the permanent magnets.

The radial magnetic induction expression at any position in space for the permanent magnet structure is obtained from (1):

$$B_r = \sum_{i=1,2,3,4,5,6} B_{ri} \tag{2}$$

where i is the number of permanent magnets.

The definition of the Lorentz force is obtained from the Lorentz force law:

$$F = \iiint_V J \times B \cdot dV \tag{3}$$

Substituting (2) into (3) gives the expressions for the electromagnetic force F and the electromagnetic torque T:

$$F = \int_{R_1}^{R_2} \int_{Z_1}^{Z_2} \int_{\phi_1}^{\phi_2} (J) B_r(r,z,\varphi) R \,\mathrm{d}\, R \,\mathrm{d}\, Z \,\mathrm{d}\, \phi \tag{4}$$

$$T = \int_{R_1}^{R_2} \int_{Z_1}^{Z_2} \int_{\phi_1}^{\phi_2} (J) B_r(r,z,\varphi) R^2 \,\mathrm{d}\, R \,\mathrm{d}\, Z \,\mathrm{d}\, \phi \tag{5}$$

where R_1 is the inner radius of the coil, R_2 is the outer radius of the coil, Z_1 is the height of the bottom surface of the coil, Z_2 is the height of the top surface of the coil, ϕ_1 is the initial angle of the coil, ϕ_2 is the stop angle of the coil.

Therefore, the analytical expressions for the electromagnetic force F and the electromagnetic torque T received by the coil assembly are:

$$\begin{cases} F = \sum_{k=1,2,3,4} F_k \\ T = \sum_{k=5,6,7,8} M_k \end{cases} \tag{6}$$

where k is the number of coils.

3. Analysis of Coupled Vibration Dynamics

A. *Uniaxial vibration model of the linear-angular vibration exciter*

In terms of uniaxial vibration, this exciter can generate uniaxial linear and angular vibrations of the moving part by relating the permanent magnet and the moving coil to each other. The moving part is connected to the exciter body, which splits the exciter into two parts: the moving part and the body. Therefore, two vibration lumped parameter models are created for the two vibration modes, as shown in Fig. 2.

The variables in Fig. 2 are as follows: M_b is the mass of the exciter body; k_b is the equivalent stiffness of the exciter body; c_b is the damping coefficient of the exciter body; x_b is the displacement change of the exciter body; M_x is the mass of the moving part; k_x is the stiffness of the moving part; c_x is the damping coefficient of the moving part; x is the displacement change of the moving part; F is the excitation force of the linear vibration; J_r is the equivalent rotational inertia of the exciter body; k_r is the equivalent torsional stiffness of the exciter body; c_r is the torsional damping coefficient of the exciter body; θ_r is the angle rotated by the exciter body; J_t is the equivalent rotational inertia of the moving part; k_t is the torsional stiffness of the moving part; c_t is the torsional damping coefficient of the moving part; T is the excitation torque of the angular vibration; θ is the angle rotated by the moving part.

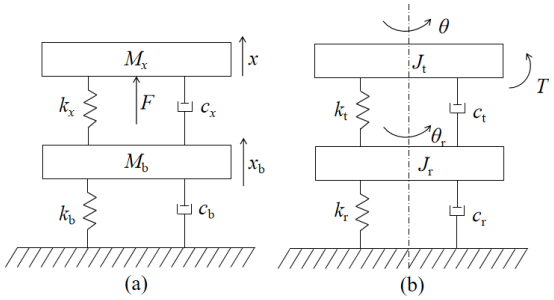

Fig. 2. The Lumped parameter model; (a) linear vibration (b) angular vibration.

Due to the large mass and the large moment of inertia of the exciter body, the excitation from the coil is not sufficient to generate motion. Therefore, the platform can be neglected in the analysis. According to Newton's second law, the differential equation for linear vibration can be obtained as follows:

$$M_x \ddot{x} + c_x \dot{x} + k_x x = F \tag{7}$$

The differential equation for angular vibration can be obtained as follows:

$$J_t \ddot{\theta} + c_t \dot{\theta} + k_t \theta = T \tag{8}$$

B. *Linear-angular coupling vibration model and analysis of coupling characteristics*

Coupled vibrations refer to the vibration input of one vibration mode (or in a generalized coordinate direction) caused by the vibration input of two (or more) vibration modes, leading to a response in another vibration mode (or in another generalized coordinate direction).

To simplify the analysis, the moving parts are represented as a uniaxial system as shown in Fig. 3. Fig. 3 shows the basic coupled vibration model of the uniaxial system consisting of a spring and a disc. This model is used to replace the vibration system of the moving part. The mass M_x, the moment of inertia J_t, the stiffness k_x, and the torsional stiffness of the disc k_t are equivalent to those of the moving part.

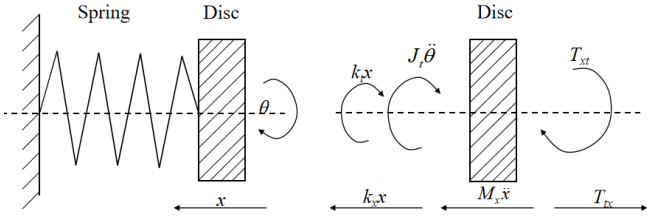

Fig. 3. The basic coupled vibration model of uniaxial system.

Fig. 3 shows that the axis undergoes torsional deformation at both positive and negative torques accompanied by axial contraction (or coupling).

Further analysis shows that the axial response contraction reaches its maximum value synchronously with the maximum torsional deformation when the axis is subjected to a positive torque. Moreover, the length of the axis is shortest when the axial contraction reaches its maximum value. Conversely, when the deformation of the axis is restored, the contraction also recovers synchronously and the length of the axis returns to its initial length when the deformation is zero. Similarly, when the axis is subjected to a negative torque, the torsional deformation and axial contraction occur synchronously and the length of the axis is shortest when the deformation reaches its maximum value. After the negative torque has disappeared, the axis returns to its initial state. When the torsional deformation of the axis goes through a cycle, it is always accompanied by cycles of axial deformation and torsional deformation that occur simultaneously, indicating that the frequency of the axial vibration is twice as high as the frequency of torsional vibration.

When the object is subjected to external loads due to its different geometric shapes and physical properties, the stiffness is nonlinear, resulting in mutual influence of different axial vibrations. We turn this non-linear stiffness into a coupling stiffness. Since there is a coupling stiffness, the torsional deformation of the moving parts, whether forward or reverse, leads to an axial coupling deformation. If the moving parts vibrate axially, the coupling stiffness also leads to torsional coupling deformation. Assuming an undamped state with a coupling stiffness of k, the function $\delta(\theta)$ is defined as the sign of the coupling stiffness. Based on the angular variation of the moving component, the direction of the axial restoring force is determined as follows: when $\theta > 0$, $\delta(\theta) = 1$, the axial restoring force is $k\theta$; when $\theta < 0$, $\delta(\theta) = -1$, the axial restoring force is $-k\theta$; when $\theta = 0$, $\delta(\theta) = 0$, the axial restoring force is 0. Therefore, the axial restoring force can be represented as $F_{tx} = \delta(\theta)k\theta$. Similarly, the torsional restoring torque can be derived as $T_{xt} = \delta(\theta)kx$.

Based on Newton's second law, the mathematical model for coupled free vibrations without damping can be derived as follows:

$$\begin{cases} J_t\ddot{\theta} + k_t\theta - \delta(\theta)kx = 0 \\ M_x\ddot{x} + k_x x - \delta(\theta)k\theta = 0 \end{cases} \tag{9}$$

$$\begin{bmatrix} J_t & 0 \\ 0 & M_x \end{bmatrix}\begin{bmatrix} \ddot{\theta} \\ \ddot{x} \end{bmatrix} + \begin{bmatrix} k_t & -\delta(\theta)k \\ -\delta(\theta)k & k_x \end{bmatrix}\begin{bmatrix} \theta \\ x \end{bmatrix} = \begin{bmatrix} 0 \\ 0 \end{bmatrix} \tag{10}$$

By applying the basic principles of solving vibration equations, the natural frequencies and mode matrix of the system can be obtained by solving (10). First, assuming that the angle and displacement are sinusoidal functions, the expressions are as follows:

$$\begin{cases} \theta(t) = \theta\sin\omega t \\ x(t) = X\sin\omega t \end{cases} \tag{11}$$

where ω is the angular frequency, t is time, X is the amplitude of the displacement and θ is the amplitude of the angle.

By substituting (11) into (10), we get:

$$\begin{bmatrix} k_t - J_t\omega^2 & -\delta(\theta)k \\ -\delta(\theta)k & k_x - M_x\omega^2 \end{bmatrix}\begin{bmatrix} \theta \\ x \end{bmatrix} = \begin{bmatrix} 0 \\ 0 \end{bmatrix} \tag{12}$$

The two natural frequencies of the system ω_{n1}^2, ω_{n2}^2 and the modal matrix **[S]** can be obtained as follows:

$$\omega_{n1、n2}^2 = \frac{1}{2}\left[\frac{k_t}{J_t} + \frac{k_x}{M_x} \pm \sqrt{\left(\frac{k_t}{J_t} - \frac{k_x}{M_x}\right)^2 + \frac{4k^2}{J_t M_x}}\right] \tag{13}$$

$$[\mathbf{S}] = \begin{bmatrix} 1 & 1 \\ \dfrac{DJ_t}{\delta(k)} & -\dfrac{\delta(k)}{DM_x} \end{bmatrix} \tag{14}$$

$$D = \frac{1}{2}\left[\frac{k_t}{J_t} - \frac{k_x}{M_x} - \sqrt{\left(\frac{k_t}{J_t} - \frac{k_x}{M_x}\right)^2 + \frac{4k^2}{J_t M_x}}\right] \tag{15}$$

As shown in (13), $k = 0$ is equivalent to the absence of coupling between the angular and linear vibrations of the system.

Based on (10) and assuming that the torque excitation of a uniaxial angular vibration system is $T\sin\omega_\theta t$, where ω_θ is the angular frequency of the torque excitation and T is the excitation amplitude, and the axial excitation is 0, the equation of motion of the system is given by:

$$\begin{bmatrix} J_t & 0 \\ 0 & M_x \end{bmatrix}\begin{bmatrix} \ddot{\theta} \\ \ddot{x} \end{bmatrix} + \begin{bmatrix} k_t & -\delta(\theta)k \\ -\delta(\theta)k & k_x \end{bmatrix}\begin{bmatrix} \theta \\ x \end{bmatrix} = \begin{bmatrix} T\sin\omega_\theta t \\ 0 \end{bmatrix} \tag{16}$$

Equation (16) is a stiffness-coupled equation. To decouple (16):

$$\begin{bmatrix} \theta \\ x \end{bmatrix} = [S]\begin{bmatrix} y_1 \\ y_2 \end{bmatrix} \tag{17}$$

Substituting (17) into (16) and multiplying both sides of the equation by $[\mathbf{S}]^{\mathbf{T}}$:

$$\begin{bmatrix} J_t + \dfrac{M_x J_t^2 D^2}{k^2} & 0 \\ 0 & J_t + \dfrac{k^2}{M_x D^2} \end{bmatrix}\begin{bmatrix} \ddot{y}_1 \\ \ddot{y}_2 \end{bmatrix} + \begin{bmatrix} k_t - 2J_t D + \dfrac{k_x J_t^2 D^2}{k^2} & 0 \\ 0 & k + \dfrac{k^2}{M_x D}\left(\dfrac{k_x}{M_x D} + 2\right) \end{bmatrix}\begin{bmatrix} y_1 \\ y_2 \end{bmatrix} = \begin{bmatrix} T\sin\omega_\theta t \\ 0 \end{bmatrix} \tag{18}$$

It can be shown that the equation has been successfully decoupled and diagonalized. Further solving leads to the steady-state solution:

$$\begin{bmatrix} y_1 \\ y_2 \end{bmatrix} = \begin{bmatrix} \dfrac{T\sin\omega_\theta t}{\left(J_t + \dfrac{M_x J_t{}^2 D^2}{k^2}\right)\left(P_{01}^1 - \omega_\theta^2\right)} \\ 0 \dfrac{T\sin\omega_\theta t}{\left(2 + \dfrac{k^2}{M_x D^2}\right)\left(P_{02}^1 - \omega_\theta^2\right)} \end{bmatrix} \tag{19}$$

where

$$P_{01}^2 = \frac{k^2\left(k_t - 2J_t D\right) + k_x J_t{}^2 D^2}{J_t + M_x J_t{}^2 D^2}$$

$$P_{02}^2 = \frac{M_x{}^2 D^2 k_t + k^2 k_x + 2k^2 M_x D}{M_x{}^2 D^2 J_t + M_x k^2}$$

Thus, according to (19), the torsional and axial response equations under the specified torque excitation can be calculated as follows:

$$\begin{bmatrix} \theta \\ \Delta x \end{bmatrix} = \begin{bmatrix} \dfrac{T\sin\omega_\theta t}{M_x J_t{}^2 D^2 + J_t k^2}\left(\dfrac{k^2}{P_{01}^2 - \omega_\theta^2} + \dfrac{M_x J_t{}^2 D^2}{P_{02}^2 - \omega_\theta^2}\right) \\ \dfrac{\delta(\theta) kDT\sin\omega_\theta t}{M_x J_t{}^2 D^2 + k^2}\left(\dfrac{1}{P_{01}^2 - \omega_\theta^2} - \dfrac{1}{P_{02}^2 - \omega_\theta^2}\right) \end{bmatrix} \tag{20}$$

Since θ has the same sign as $\sin\omega_\theta t$ in (20), the axial displacement Δx caused by the torsional vibration can be obtained as follows:

$$\Delta x = \left|\sin\omega_\theta t\right| \times \frac{kDT}{M_x J_t D^2 + k^2}\left(\frac{1}{P_{01}^1 - \omega_\theta^2} - \frac{1}{P_{02}^1 - \omega_\theta^2}\right) \tag{21}$$

Equation (21) can be extended to a Fourier series as follows:

$$\left|\sin\omega_\theta t\right| = \frac{4}{\pi}\left(\frac{1}{2} - \frac{1}{3}\cos 2\omega_\theta t - \frac{1}{15}\cos 4\omega_\theta t - \cdots\cdots\right) \tag{22}$$

$$\begin{aligned} \Delta x = {} & \frac{4kDT}{\pi\left(M_x J_t D^2 + k^2\right)}\left(\frac{1}{P_{01}^1 - \omega_\theta^2} - \frac{1}{P_{02}^1 - \omega_\theta^2}\right) \\ & \times\left(\frac{1}{2} - \frac{1}{3}\cos 2\omega_\theta t - \frac{1}{15}\cos 4\omega_\theta t - \cdots\cdots\right) \end{aligned} \tag{23}$$

In (23), the Fourier expansion of the axial displacement from (22) is obtained. It can be observed that there are high-frequency components in the axial vibration response caused by torque excitation, of which the 2nd harmonic component has a larger and more prominent amplitude, while the 4th harmonic component has a much smaller amplitude than the 2nd harmonic component.

Based on (10), a uniaxial vibration system is subjected to an excitation of $F\sin\omega_x t$, where ω_x is the angular frequency of the axial excitation and F is the excitation amplitude. The torsional excitation is zero and the equation of motion is as follows:

$$\begin{bmatrix} J_t & 0 \\ 0 & M_x \end{bmatrix}\begin{bmatrix} \ddot{\theta} \\ \ddot{x} \end{bmatrix} + \begin{bmatrix} k_t & -\delta(\theta)k \\ -\delta(\theta)k & k_x \end{bmatrix}\begin{bmatrix} \theta \\ x \end{bmatrix} = \begin{bmatrix} 0 \\ F\sin\omega_x t \end{bmatrix} \tag{24}$$

Using the same method, the axial and torsional response equations under the specified axial excitation can be obtained as follows:

$$\begin{bmatrix} x \\ \Delta\theta \end{bmatrix} = \begin{bmatrix} \dfrac{F\sin\omega_x t}{J_t M_x{}^2 D^2 + M_x k^2}\left(\dfrac{J_t M_x D^2}{P_{01}^2 - \omega_x^2} + \dfrac{k^2}{P_{02}^2 - \omega_x^2}\right) \\ \dfrac{\delta(\theta) kDF\sin\omega_x t}{M_x J_t D^2 + k^2}\left(\dfrac{1}{P_{01}^2 - \omega_x^2} - \dfrac{1}{P_{02}^2 - \omega_x^2}\right) \end{bmatrix} \tag{25}$$

Equation (25) shows that the magnitude of the coupled torsional vibration response $\Delta\theta$ caused by axial excitation depends on the initial state of the exciter torque angle. When $\theta(t{=}0) = 0$, $\delta(\theta) = 0$, then $\Delta\theta = 0$. In other words, an axial excitation will not induce any coupled torsional vibration response.

By adding both the axial excitation $F\sin\omega_x t$ and the torsional excitation $T\sin\omega_\theta t$ to (10), the vibration equation for the synchronized output of the linear-angular vibration exciter can be obtained as follows:

$$\begin{cases} M_x\ddot{x} + k_x x - \delta(\theta)k\theta = F \\ J_t\ddot{\theta} + k_t\theta - \delta(\theta)kx = T \end{cases} \tag{26}$$

$$\begin{bmatrix} J_t & 0 \\ 0 & M_x \end{bmatrix}\begin{bmatrix} \ddot{\theta} \\ \ddot{x} \end{bmatrix} + \begin{bmatrix} k_t & -\delta(\theta)k \\ -\delta(\theta)k & k_x \end{bmatrix}\begin{bmatrix} \theta \\ x \end{bmatrix} = \begin{bmatrix} T\sin\omega_\theta t \\ F\sin\omega_x t \end{bmatrix} \tag{27}$$

It can be deduced that the vibration response equation under axial-torsional excitation is as follows:

$$\begin{bmatrix} \theta \\ x \end{bmatrix} = \begin{bmatrix} \dfrac{T\sin\omega_\theta t}{M_x J_t{}^2 D^2 + J_t k^2}\left(\dfrac{k^2}{P_{01}^2 - \omega_\theta^2} + \dfrac{M_x J_t{}^2 D^2}{P_{02}^2 - \omega_\theta^2}\right) \\ + \dfrac{\delta(\theta) kDF\sin\omega_x t}{M_x J_t D^2 + k^2}\left(\dfrac{1}{P_{01}^2 - \omega_x^2} - \dfrac{1}{P_{02}^2 - \omega_x^2}\right) \\ \dfrac{F\sin\omega_x t}{J_t M_x{}^2 D^2 + M_x k^2}\left(\dfrac{J_t M_x D^2}{P_{01}^2 - \omega_x^2} + \dfrac{k^2}{P_{02}^2 - \omega_x^2}\right) \\ + \dfrac{\delta(\theta) kDT\sin\omega_\theta t}{M_x J_t{}^2 D^2 + k^2}\left(\dfrac{1}{P_{01}^2 - \omega_\theta^2} - \dfrac{1}{P_{02}^2 - \omega_\theta^2}\right) \end{bmatrix} \tag{28}$$

Equation (28) shows that the displacement and angular responses obtained under the influence of axial-torsional excitation are actually the linear superposition of their respective responses under individual excitation.

4. PARAMETER IDENTIFICATION MODEL BASED ON ELECTROMECHANICAL ANALOGY

A. Electromechanical analogy model

The electromagnetic linear-angular vibration exciter is a mechatronic system. By applying the principle of electromechanical analogy, the vibration system can be

converted into a circuit diagram, which allows the use of the established theory of circuit analysis to simplify the analysis process. Using the impedance-based electromechanical analogy principle, the vibration system can be converted into a circuit diagram. The dynamic parameters of the mechanical system and the electrical parameters of the circuit system are modeled analogously. This results in the uniaxial vibration electromechanical analogy model, as shown in Fig. 4.

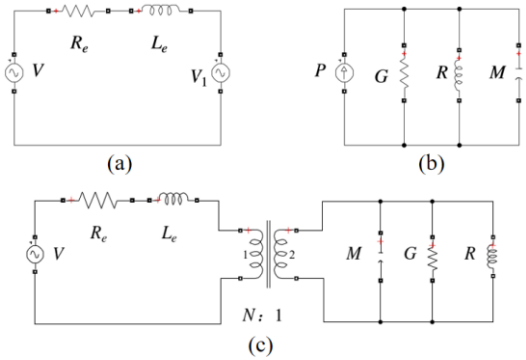

Fig. 4. The uniaxial vibration electromechanical analogy model; (a) linear (b) angular (c) coupled linear and angular.

Combining the model from Fig. 4(a) and Fig. 4(b) leads to the uniaxial vibration electromechanical analogy model, as shown in Fig. 4(c). Since the differential equation structure of the linear and angular vibration of the exciter is the same, both types of vibration have the same electromechanical analogy model. The mechanical parameters in the model are represented as sets, each containing a linear vibration parameter and an angular vibration parameter. Specifically, M corresponds to the mass of the moving component M_x, and the moment of inertia J_t; R corresponds to the axial and torsional stiffness (stiffness is the reciprocal of compliance) $1/k_x$ and $1/k_t$, respectively, of the moving component; G corresponds to the axial and torsional damping (damping is the reciprocal of resistance), $1/c_x$ and $1/c_t$, of the moving component, respectively; N corresponds to the linear vibration force factor N_1, and the angular vibration force factor N_2; P corresponds to the linear vibration excitation force F, and the angular vibration excitation torque T. The electrical parameters of the circuit include the coil resistance R_e, the coil inductance L_e and the coil voltage V.

B. Uniaxial vibration parameter identification model

The dynamic parameters of the exciter can be determined by analyzing its response around the resonant frequency. According to Fig. 4, the impedance formula Z can be determined as follows:

$$Z = R_e + GN^2\left[\frac{j\omega R}{j\omega R + \left(1-\omega^2 MR\right)G}\right] \tag{29}$$

According to the impedance formula, the imaginary part of the impedance is equal to 0 and the modulus of the admittance is the largest, when $\omega = \omega_1 = 1/\sqrt{MR}$, i.e. the frequency is the resonance frequency. Taking linear vibration as an example, the resonant frequency under load $\omega = \omega_2 = 1/\sqrt{(M+m)R}$ can be obtained by conducting a load experiment by setting a standard mass block with the mass m on the workbench. The values for mass and stiffness can be calculated based on the unloaded and loaded resonant frequencies of the linear vibration, and the calculation formula is as follows:

$$M_x = \frac{m\omega_2^2}{\omega_1^2 - \omega_2^2} \tag{30}$$

$$k_x = \frac{1}{R} = M\omega_1^2 \tag{31}$$

To obtain the value of the force factor N, it is necessary to measure the current I in the coil and the linear acceleration signal A of the moving part in the linear vibration mode of the exciter. According to Ampere's law $F = IBL$, the calculation formula for the force factor N_1 in linear vibration is as follows:

$$F = M_x \times A = IN_1 \tag{32}$$

$$N_1 = \frac{\left(M_x \times A\right)}{I} \tag{33}$$

By performing an FFT analysis of the voltage, current, and acceleration signals, the impedance value at the resonant frequency can be obtained. According to the impedance formula equations (29), the imaginary part of the impedance is zero when the moving part is at the resonant frequency. The formula for calculating the damping coefficient c_x is as follows:

$$c_x = \frac{1}{G} = \frac{N_1^2}{Z - R_e} \tag{34}$$

To calculate the values of rotational inertia J_t, torsional stiffness k_t and damping coefficient c_t for angular vibration mode, experimental data must be collected for the exciter, which should be substituted into (30) ~ (34) together with the rotational inertia value J_m of the standard mass block.

C. Coupled vibration parameter identification model

The exciter can output linear and angular vibration signals synchronously. Based on its operating principle, a coupled vibration equivalent electromechanical analog model can be created, as shown in Fig. 5. The upper part of the model represents the linear vibration part and the lower part represents the angular vibration part.

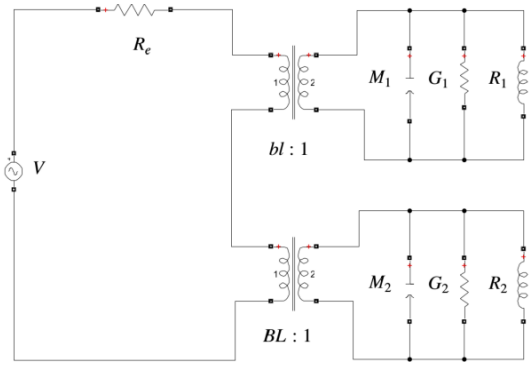

Fig. 5. Coupled vibration electromechanical analog model.

The analysis of (28) shows that the coupled vibration has no effect on the torsional vibration under ideal conditions. Therefore, $M_2 = J_t$, $R_2 = 1/k_t$, and $G_2 = 1/c_t$ in the model. Based on the model, the impedance expression Z_1 can be determined as follows:

$$Z_1 = R_e + G_1 N_1^2 \left[\frac{j\omega R_1}{j\omega R_1 + \left(1 - \omega_3^2 M_1 R_1\right) G_1} \right] + G_2 N_2^2 \left[\frac{j\omega R_2}{j\omega R_2 + \left(1 - \omega_4^2 M_2 R_2\right) G_2} \right] \tag{35}$$

The expression for the coupling stiffness k can be obtained by combining the natural frequency of the coupled linear vibration, ω_3 (corresponding to ω_{n1}), with $\omega_1 = 1/\sqrt{MR}$ and (35) as follows:

$$k = \sqrt{\left(k_t - J_t \omega_3\right)\left(k_x - M_x \omega_3\right)} \tag{36}$$

Since the value of the coupling stiffness k is small compared to the motion part stiffness k_x, it can be ignored. Therefore, $M_1 = M_x$ and $R_1 = 1/k_x$ in the model. However, the coupling vibration causes a change in the damping value of the linear vibration, so that G_1 is the coupled force conduction, the reciprocal of the coupling vibration damping c_1. According to the impedance formula (35), the imaginary part of the impedance of the linear vibration part of the model is 0 when $\omega_3 = 1/\sqrt{M_1 R_1}$. The impedance value of the angular vibration part is much smaller than that of the linear vibration part, so it can be ignored. Consequently, the value of the coupling linear vibration damping c_1 can be determined. The calculation formula is:

$$c_1 = \frac{1}{G_1} = \frac{N_1^2}{Z_1 - R_e} \tag{37}$$

5. SIMULATION VERIFICATION

A. *Validation of coupled vibration characteristics by simulation*

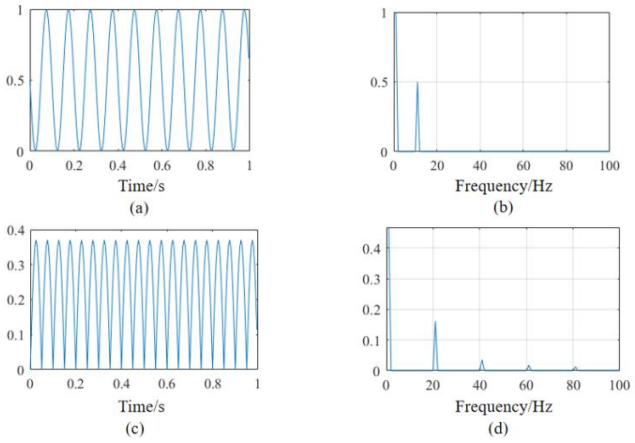

Fig. 6. Time-domain and corresponding frequency spectrum for the angular vibration: (a) angular vibration time-domain curve, (b) angular excitation spectrum, (c) displacement response time-domain curve, (d) displacement response spectrum.

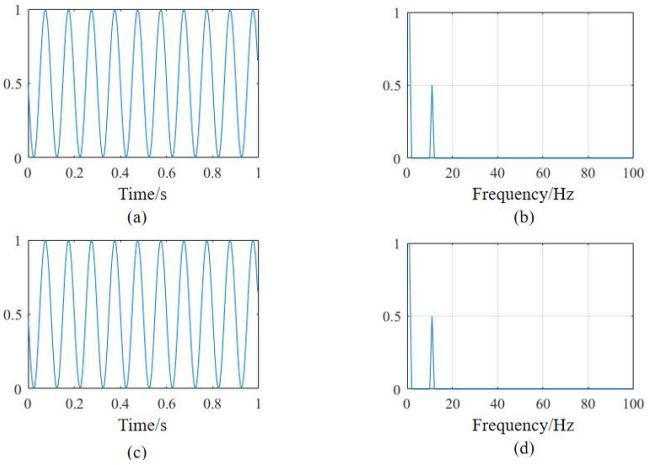

Fig. 7. Time-domain and corresponding frequency-domain spectra for the linear vibration: (a) linear vibration time-domain curve, (b) linear vibration excitation spectrum, (c) angle response time-domain curve, (d) angle response spectrum.

To verify the phenomenon of coupled vibration harmonics, $m = 1$ kg, $J = 1$ kg m^2, $k_t = 5.0$ N m^{-1}, $k_x = 0.8$ N m^{-1} and $k = 2$ N m^{-1} are set in the simulation, with the excitation frequency set to 10 Hz. To facilitate comparison and observation, the excitation amplitude is dimensionless, with the y-axis of the simulation curve representing the amplitude without unit. By simulation calculation, the time-domain response curve and the corresponding results of the frequency spectrum analysis of the vibration system under the excitation are obtained, as shown in Fig. 6 and Fig. 7.

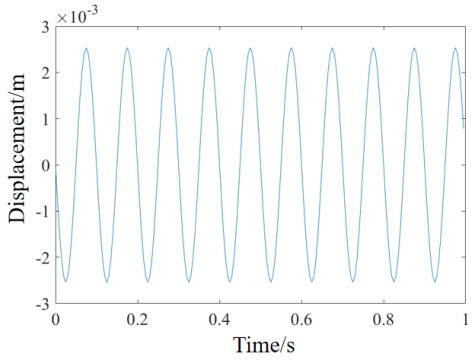

Fig. 8. The axial displacement curve under the linear vibration excitation.

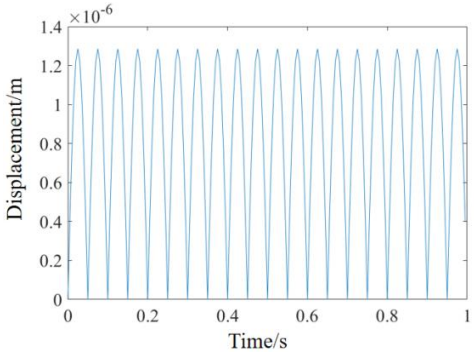

Fig. 9 The axial response displacement curve under the angular vibration excitation.

Fig. 8 and Fig. 9 show the displacement curves under linear vibration excitation and the displacement response curves under angular vibration excitation, respectively. The comparison of the two curves shows that the coupled axial displacement caused by the angular vibration excitation is much smaller than the displacement caused by the linear vibration excitation itself, indicating that the coupling effect of the angular vibration on the linear vibration can be ignored.

B. Verification of the parameter identification model

In this paper the effectiveness of the proposed method is verified using numerical simulation examples. The excitation in the vibration differential equation is simplified to a sinusoidal signal with time t as a variable, i.e., $F = A_0 sin\omega t$, $T = B_0 sin\omega t$, where A_0 and B_0 are the excitation amplitudes of linear vibration and angular vibration, respectively, and ω is the angular frequency. The excitation amplitudes are set to $A_0 = 10$ and $B_0 = 0.2$, and the angular frequency $\omega = 2\pi$. A standard block with a mass of $m = 4$ kg and a moment of inertia of $J_m = 0.4$ (kg m^2) is added. The dynamic parameters of the exciter are set with preset value parameters, and a simulation model is created based on the vibration differential equation to obtain the acceleration signals under specified excitation for both the unloaded and loaded cases. The frequency response curves of the acceleration signals obtained by FFT analysis are shown in Fig. 10. Fig. 10(a), Fig. 10(b) and Fig. 10(c) correspond to the frequency response curves of linear vibration, angular vibration, and coupled vibration, respectively. The corresponding resonant frequencies are determined from the frequency response curves and converted into angular frequencies, as shown in Table 1.

Table 1. The vibration resonance frequency.

Parameter	Frequency [Hz]	Angular frequency [rad·s-1]	Frequency [Hz]	Angular frequency [rad·s-1]
Linear vibration	35.50	223.05	25.23	158.52
Angular vibration	78.20	491.34	55.80	350.60
Coupled linear vibration	35.60	223.68	25.50	160.22

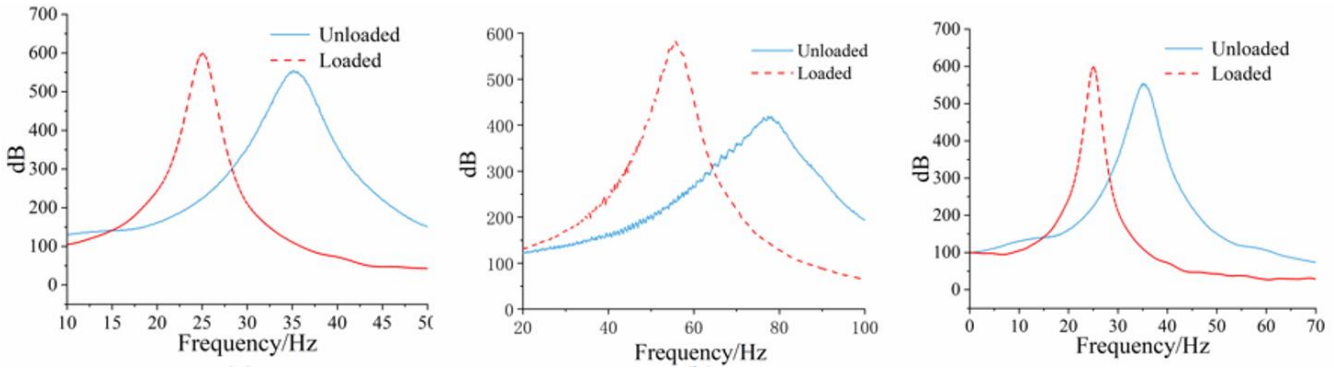

Fig. 10. The vibration frequency response curve: (a) linear vibration, (b) angular vibration, (c) coupled vibration.

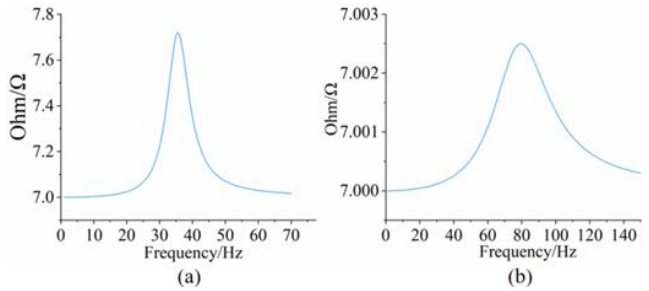

Fig. 11. The impedance-frequency curve: (a) linear vibration, (b) angular vibration.

The values of resistance and force factor are defined with the resistance $Re = 7\ \Omega$ and the force factor $N_1 = 12$ for linear vibration or the force factor $N_2 = 0.5$ for angular vibration. The simulation of the impedance-frequency graph of linear and angular vibrations is carried out using an impedance model, as shown in Fig. 11. The graph shows that the impedances of the linear and angular vibrations reach their maximum values at the resonant frequency, which are 7.7182 and 7.0025, respectively. By substituting these impedance values and resonant frequency values into the parameter identification model, the identification results are obtained, as shown in Table 2.

Table 2. Comparison of identification results.

Parameter	Preset value	Estimated value	Error [%]
M [kg]	4	4.0824	2.1
J [kg·m²]	0.4	0.4140	3.5
K_x [N·m^{-1}]	2.0×10^5	2.0311×10^5	1.6
K_t [N·m^{-1}]	1.0×10^5	1.0019×10^5	1.9
c_x [N/(m·s^{-1})]	200	200.55	0.3
c_t [N/(m·s^{-1})]	100	100.40	0.4
K [N·m^{-1}]	5000	5017.08	3.4

Comparison of the frequency response curve and the impedance-frequency curve shows that the impedance reaches its maximum value at the resonant frequency, which

is consistent with the analysis in the previous section. As shown in Table 2, under the specified excitation, the estimated parameter values obtained by the identification model are almost identical to the given values, and the relative error of each parameter identification is within 1%. It can be concluded that the parameter identification model can achieve high-precision parameter identification results under noise-free conditions.

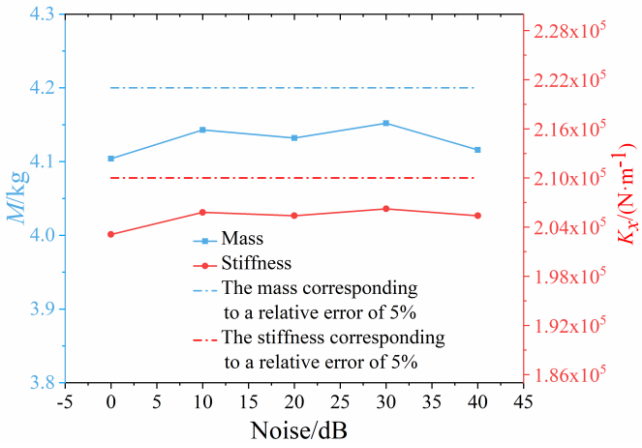

Fig. 12. Comparison of noise identification results.

To investigate the effect of noise on the identification results, white noise with signal-to-noise ratios (SNRs) of 20 dB and 30 dB was added to the excitation source of the linear vibration as an example. Numerical simulations were carried out to determine the resonant frequencies at different noise levels, and the identification results are shown in Fig. 12.

The numerical simulation results show that the identification results are in good agreement with the set values regardless of the presence of noise, and the relative error of each parameter identification is within 5%. Thus, it can be seen that the proposed model can achieve high-precision parameter identification results under both noise-free or noisy conditions.

This identification method determines the unloaded and loaded resonant frequencies of the moving part by placing an additional standard mass block on the moving table. To verify the influence of the parameters of the additional mass block on the identification accuracy, various sizes of additional masses are set and simulated. Using linear vibration as an example, the additional mass values m_1, m_2, m, m_3, and m_4 are set, where $m_1 = 0.5$ kg, $m_2 = 2$ kg, $m = 4$, $m_3 = 8$ kg and $m_4 = 12$ kg. The corresponding resonant frequencies are determined by simulation and the identification results are shown in Table 3.

From the identification results in Table 3, it can be seen that the relative errors in the identification of m_1, m_2, and m_4 are larger than those of m and m_3. This indicates that changes in the mass value of the additional standard block have a certain impact on the identification accuracy. Furthermore, excessively large or small additional masses increase the difficulty in detecting and analyzing acceleration signals.

Table 3. Identification results under load conditions.

Additional mass	Total mass of moving components [M/kg]			Stiffness of moving components [K_x/(N·m^{-1})]		
	Preset value	Estimated value	Error [%]	Preset value	Estimated value	Error [%]
m	4	4.0824	2.1	2.0×10^5	2.0311×10^5	1.6
m_1	4	4.2639	6.6	2.0×10^5	2.1441×10^5	7.2
m_2	4	4.1402	3.5	2.0×10^5	2.0420×10^5	2.1
m_3	4	4.1281	3.2	2.0×10^5	2.0479×10^5	2.4
m_4	4	4.1558	3.9	2.0×10^5	2.0462×10^5	2.3

6. CONCLUSION

In this paper, the coupling vibration characteristics of an electromagnetic linear-angular vibration exciter are analyzed by creating a theoretical model. The theoretical expressions of electromagnetic force and torque and the coupling vibration equation of the exciter are derived to analyze its coupling vibration characteristics. Based on the electromechanical analogy principle, the proposed dynamic parameter identification method is suitable and effective.

The displacement response caused by angular vibration excitation has high-order harmonics, while the angle response frequency caused by linear vibration excitation is identical to the original excitation frequency. This phenomenon confirms the coupling vibration characteristics that the angular vibration affects the linear vibration. The coupling displacement caused by the coupling vibration is much smaller than that caused by the linear vibration excitation itself, indicating that the influence of the coupling vibration is negligible.

The identification results of the proposed method under noise-free and noisy conditions are almost consistent with the given values, and the relative errors of each parameter identification are within 5%, which proves the method's accuracy and noise resistance. Changing the mass value of the additional standard block in the model has a certain impact on the identification accuracy.

ACKNOWLEDGMENT

This research is sponsored by the Zhejiang Provincial Natural Science Foundation (LY21E050017) in China, and in part by the Ningbo Key Research and Development Program under Grant 2022Z092.

REFERENCES

[1] Takiguchi, M., Sugimoto, H., Kurihara, N., Chiba, A. (2015). Acoustic noise and vibration reduction of SRM by elimination of third harmonic component in sum of radial forces. *IEEE Transactions on Energy Conversion*, 30 (3), 883-891. https://doi.org/10.1109/TEC.2015.2401398

[2] Zhai, G. D., Yang, X., Lv, Q. (2021). A calibration system of resonant high-acceleration and metrological traceability. *Measurement Science and Technology*, 32 (12), 125904. https://doi.org/10.1088/1361-6501/ac28d1

[3] Guo, Y. Q., Li, Z. Y., Yang, X. L. (2021). Research on structure design of mechanical shaking table and its waveform recurrence performance test. *Aerospace Shanghai*, 38 (1), 53-60. https://doi.org/10.19328/j.cnki.1006-1630.2021.01.007

[4] Parsons, M. G. (1983). Mode coupling in torsional and longitudinal shafting vibrations. *Marine Technology and SNAME News*, 20 (3), 257-271. https://doi.org/10.5957/mt1.1983.20.3.257

[5] Li, Z., Yan, X., Qin, L. (2015). Robust global sliding model control for water-hull-propulsion unit interaction systems-part 2: Model validation. *Technical Gazette*, 22 (2), 465-473. https://doi.org/10.17559/TV-20141208054604

[6] Huang, Q. W, Zhang, C., Jin, Y., Yuan, C. Q., Yan, X. P. (2015). Vibration analysis of marine propulsion shafting by the coupled finite element method. *Journal of Vibroengineering*, 17 (7), 3392-3403. https://www.extrica.com/article/15959

[7] Huang, Q. W., Yan, X. P., Wang, Y. K., Zhang, C., Wang, Z. H. (2017). Numerical modeling and experimental analysis on coupled torsional-longitudinal vibrations of a ship's propeller shaft. *Ocean Engineering*, 136, 272-282. https://doi.org/10.1016/j.oceaneng.2017.03.017

[8] Ni, H. P., Zhang, C. R., Hu, T. L., Wang, T., Chen, Q. Z., Chen, C. (2019). A dynamic parameter identification method of industrial robots considering joint elasticity. *International Journal of Advanced Robotic Systems*, 16 (1). https://doi.org/10.1177/1729881418825217

[9] Kwon, J., Choi, K., Park, F. C. (2021). Kinodynamic model identification: A unified geometric approach. *IEEE Transactions on Robotics*, 37 (4), 1100-1114. https://doi.org/10.1109/TRO.2020.3047515

[10] Ng, C.-T., Au, S.-K. (2018). Mode shape scaling and implications in modal identification with known input. *Engineering Structures*, 156, 411-416. https://doi.org/10.1016/j.engstruct.2017.11.017

[11] Wen, Q., Hua, X. G., Chen, Z. Q., Guo, J. M., Niu, H. W. (2017). Modal parameter identification of a long-span footbridge by forced vibration experiments. *Advances in Structural Engineering*, 20 (5), 661-673. https://doi.org/10.1177/1369433217698322

[12] Xia, J. N., Song, H. W. (2017). Modal parameter identification of structure under base excitation using vibration test data. *Proceedings of the Institution of Mechanical Engineers Part G: Journal of Aerospace Engineering*, 231 (8), 1428-1450. https://doi.org/10.1177/0954410016652919

[13] López-Martínez, J., Martínez, J. C., García-Vallejo, D. Alcayde, A., Montoya, F. G. (2021). A new electromechanical analogy approach based on electrostatic coupling for vertical dynamic analysis of planar vehicle models. *IEEE Access*, 9, 119492-119502. https://doi.org/10.1109/ACCESS.2021.3108488

[14] Saraswat, A., Tiwari, N. (2017). Modeling and study of nonlinear effects in electrodynamic shakers. *Mechanical Systems and Signal Processing*, 85, 162-176. https://doi.org/10.1016/j.ymssp.2016.07.025

[15] Tiwari, N., Puri, A., Saraswat, A. (2017). Lumped parameter modelling and methodology for extraction of model parameters for an electrodynamic shaker. *Journal of Low Frequency Noise, Vibration and Active Control*, 36 (2), 99-115. https://doi.org/10.1177/0263092317693511

Received June 05, 2023
Accepted January 09, 2024